Inertial geometric quantum logic gates

D.Turyansky¹, O. Ovdat², R. Dann³, Z. Aqua², R. Kosloff³, B. Dayan², and A.Pick¹

We present rapid and robust protocols for single- and two-qubit quantum logic gates. Our gates are based on geometric phases acquired by instantaneous eigenstates of a slowly accelerating "inertial" Hamiltonian. We begin by defining conditions for inertial population transfer and, then, find pulse shapes that meet these conditions. We use those pulses to perform inertial quantum logic gates and optimize their performance. As an application of our approach, we propose an implementation of our protocol with 87Rb atoms and analyze the effect of polarization and leakage errors. Our approach can be extended beyond geometric gates and is useful for speeding up adiabatic quantum computation protocols.

1 Introduction

Rapid high-fidelity quantum logic gates are essential for large-scale atom-based quantum computers [1, 2, 3]. State-of-the-art experiments can reach fidelities of 99% and 95% for single-qubitand two-qubit gates respectively [3, 4, 5], bringing them closer but still not reaching the required threshold values for fault-tolerant quantum computation [6]. Further improving these abilities is a key goal in quantum computation research. Atomic qubits are typically encoded in long-lived hyperfine states and transitions between them are driven indirectly via excited states. Physical processes that limit gate fidelity include depolarization and dephasing, induced by spontaneous emission from the excited states, and imperfections in the control fields that implement the gate. An elegant approach to combat these issues involves adiabatic following of "dark states:" By slowly varying the control fields, the system adheres to a dark combination of the long lived states, which is decoupled from radiation and is, therefore, protected from incoherent emission. This principle forms the basis of stimulated Raman adiabatic passage (STIRAP) [7] and geometric quantum logic gates [8]. The outcome of such protocols depends only on the geometric phase acquired by the dark eigenstate and on the final state of the system. Hence, it is robust to certain perturbations (i.e., those that do not affect the geometric phase or final state). For the system to adhere to the dark state, the protocol must be sufficiently slow, limiting the computational speed.

Contribution

Quantum computation errors can be reduced by using adiabatic protocols, which involve slow manipulation of the qubits. However, the slowness of these protocols limits their performance. In this work, we propose an alternative approach that achieves the same level of robustness by using inertial protocols [9, 10]. Unlike adiabatic protocols, these protocols do not rely on slow manipulation, but rather utilize slow acceleration to achieve robustness. To demonstrate the full power of this approach, we develop an algorithm that finds optimal protocols for universal quantum logic gates.

Many efforts have focused on speeding up adiabatic schemes and increasing their fidelity while

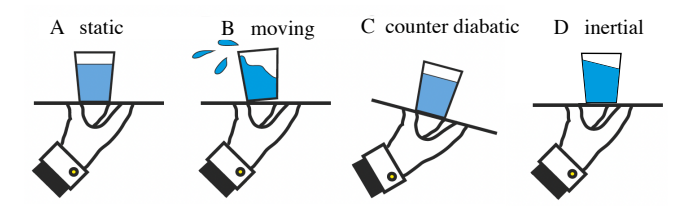


Fig. 1: Inertial motion versus transitionless driving. (a–c) Transitionless driving (borrowed from [11]): A moving waiter carrying a cup may tilt the tray to create a counter-diabatic force and prevent spilling. (d) Inertial motion: In the frame of the cup, the water stays in place as long as the acceleration is kept small.

¹Department of Applied Physics, The Hebrew University of Jerusalem, Jerusalem 9190401, Israel

²Department of Chemical Physics, Weizmann Institute of Science, Rehovot 76100, Israel

³The Institute of Chemistry, The Hebrew University of Jerusalem, Jerusalem 9190401, Israel

maintaining their robustness [7]. A seminal paper by Berry [12] showed that adiabatic approximations can be made exact and rapid by introducing appropriate fields that counteract diabatic transitions, resulting in "transitionless driving." This idea is illustrated in Fig. 1(a-c) (borrowed from [11]), where a cup of a running waiter is being tilted to avoid spilling. An application of this approach to STIRAP successfully produced a high-fidelity rapid and robust population transfer protocol [13, 14, 15, 16, 17, 18]. Recent work presents a prescription for finding improved transitionless-driving protocols with inherently small counter-diabatic terms [19]. Since such protocols differ only slightly from the adiabatic protocols, they are often easy to implement. Although significantly improving conventional STIRAP [20], errors in the implementation of the counter-diabatic Hamiltonian terms translate into errors in the eigenstate and, therefore, limit the gate fidelity and speed. Alternatively, one can try to improve adiabatic protocols by optimizing the parameters of analytic adiabatic pulses [21, 22]. For example, in Ref. [21], optimized pulses were used to reduce diabatic errors below the threshold required for fault tolerant quantum computation (using an idealized theoretical model system). Despite its simplicity, this approach is limited in its ability to improve performance in a general setting. To push these results further, one needs to resort to bruteforce optimization methods, such as quantum optimal control (QOCT) [23, 24, 25]. It remains a challenge to find optimal solutions that are both practical and globally optimal. In this work, we use the recent "inertial theorem" [9, 10] to find optimal STIRAP pulses with simple-shaped pulses. By transforming the Hamiltonian into an appropriate "inertial frame" and rescaling the time coordinate, we find solutions that are adiabatic in the new frame but may vary rapidly in the original frame. This concept is illustrated in Fig. 1(d), where the cup of a running waiter does not spill as long as the waiter's acceleration is small. We use inertial solutions as an initial guess for QOCT and impose adiabaticity and inertiality constraints in the optimization algorithm.

We use the optimized protocols to improve quantum logic gates that use geometric phases acquired during cyclic evolution [26, 27]. Specifically, these protocols employ tripod-level atoms,

as proposed in [8] and demonstrated experimentally in [28]. Our approach is generic and can be used to improve additional adiabatic protocols. For example, a recent proposal associates SU(2)rotations with fixed ratios between the pump and Stokes STIRAP fields [29]; The gate fidelity is limited by diabatic transitions and, hence, can be improved by our approach. Another example is a STIRAP motivated approach for Grover's search algorithm, which finds a marked item in an unsorted list [30]. Finally, adiabatic protocols are used in quantum simulated annealing, where a system is adiabatically brought into a final state that solves a complex computational problem. Efforts have concentrated on speeding up quantum annealing, for example, by using a variational transitionless-driving approach [11]. Based on our present work, inertial solutions are expected to be useful for improving such protocols.

2 Inertial evolution

The inertial theorem utilizes a timescale separation between variables to obtain approximate solutions for the system's dynamics under rapid external driving [9]. The theorem is derived in Liouville space – the vector space of operators on the Hilbert space. Starting with the Heisenberg equations of motion for the system operators, one identifies a suitable time-dependent operator basis for which the equations of motion vary on two timescales. By rescaling the generalized time coordinates, one can eliminate the fast dynamics and, then, identify new dynamical symmetries – operators whose Heisenberg representation is independent of time. These symmetries enable the construction of approximate analytic solutions. For the system considered in this paper, the construction in Liouville space inspires an equivalent formulation in Hilbert space.

Let $|\psi\rangle$ satisfy the Schrödinger equation, $i\hbar \partial |\psi\rangle/\partial t = H(t)|\psi\rangle$, and introduce the eigenvalue decomposition of the Hamiltonian,

$$H(t) = P\Lambda P^{-1},\tag{1}$$

where P and Λ are instantaneous matrices of eigenvectors and eigenvalues of the Hamiltonian H(t) respectively. Let us use the eigenvector matrix to define the state $|\tilde{\psi}\rangle = P|\psi\rangle$, which satis-

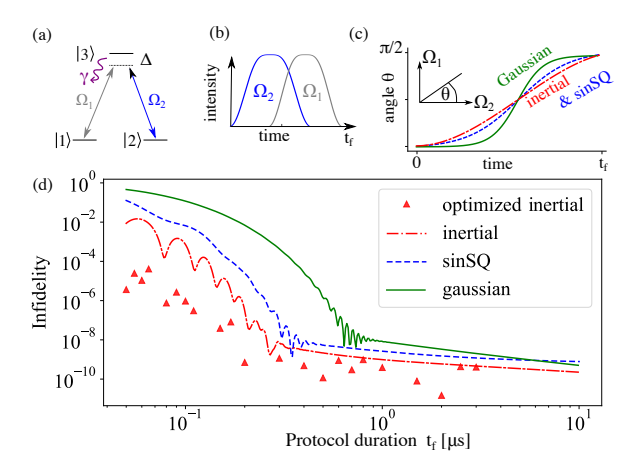


Fig. 2: Inertial and conventional STIRAP. (a-b) Population is transferred from $|1\rangle$ to $|2\rangle$ by applying the pulse Ω_2 and then $\Omega_1.$ (c) Three pulse shapes are analyzed: Gaussian (solid green), sine squared (dashed blue) and inertial (dash-dot red). Pulses are parameterized by the plotted angle, $\theta(t) \equiv \tan^{-1}(\Omega_1/\Omega_2).$ (d) Infidelity as a function of protocol duration for the three pulse shapes. Parameters: $\Delta=50 \rm MHz$, maximal intensity $\Omega=50 \rm MHz$ and $\gamma/2\pi=6 \rm \, MHz.$ Optimized results shown by triangles.

fies

$$i\hbar \frac{\partial |\tilde{\psi}\rangle}{\partial t} = \left(P^{\dagger}HP - i\hbar P^{\dagger}\frac{\partial P}{\partial t}\right)|\tilde{\psi}\rangle \equiv \tilde{H}|\tilde{\psi}\rangle. \tag{2}$$

(Note that Eq. (2) is valid for any matrix P, not necessarily the eigenvector matrix.) Inertial frames are those in which \tilde{H} can be written in the form

$$\tilde{H} = \Omega(t) \mathbb{M}(\chi), \tag{3}$$

where $\Omega(t)$ is a possibly rapidly varying scalar while χ is nearly stationary. Introducing a rescaled time coordinate, $\tau = \int_0^t \Omega(t')dt'$, we obtain the inertial frame Schrödinger equation

$$i\hbar \frac{\partial |\tilde{\psi}\rangle}{\partial \tau} = \mathbb{M}(\chi)|\tilde{\psi}\rangle.$$
 (4)

The solutions, $|\tilde{\psi}(\tau)\rangle$, can be approximated by adiabatically following the eigenstates of M. The validity condition is that M is slowly varying compared to its energy gap. We will see that for STIRAP, this condition amounts to constraining the second-order temporal derivative of the control parameters (i.e., acceleration), versus the adiabatic condition constraining the velocity.

3 The inertial STIRAP protocol

Consider a three-level system driven by two fields as shown in Fig. 2(a). The goal of the protocol is to transfer population between the ground states, from $|1\rangle$ to $|2\rangle$, without populating the third state, $|3\rangle$. Assuming that the fields are both detuned from the atomic transition by Δ , the Hamiltonian of this system is

$$H = \Omega_1 |1\rangle\langle 3| + \Omega_2 |2\rangle\langle 3| + \text{h.c.} + \Delta |3\rangle\langle 3|$$

= $\Omega |B\rangle\langle 3| + \Omega^* |3\rangle\langle B| + \Delta |3\rangle\langle 3|,$ (5)

where the "bright" superposition state is defined as: $|B\rangle \equiv (\Omega_1|1\rangle + \Omega_2|2\rangle)/\Omega$, with $\Omega \equiv \sqrt{\Omega_1^2 + \Omega_2^2}$. The orthogonal "dark" state, $|D\rangle \equiv (\Omega_2|1\rangle - \Omega_1|2\rangle)/\Omega$, is an eigenvector of H with eigenvalue 0. In the adiabatic limit, a system initialized in $|D\rangle$ remains in $|D\rangle$. Therefore, to transfer population from $|1\rangle$ to $|2\rangle$ by following the dark state, one needs to first turn on only Ω_2 , then turn it off slowly and turn on Ω_1 . This "counter-intuitive" pulse sequence is shown in Fig. 2(b).

Next, we present conditions for finding inertial STIRAP solutions. We introduce the parameterization

$$\Omega_1 = \Omega(t) \sin \theta(t)$$
 $\Omega_2 = \Omega(t) \cos \theta(t)$. (6)

The conditions are

(i)
$$\theta(0) = 0$$
 , $\theta(t_f) = \pi/2$
(ii) $\dot{\theta}(0) = \dot{\theta}(t_f) = 0$,
(iii) $\ddot{\theta} \ll \Omega^4/\Delta^2$. (7)

where t_f is the protocol duration. Condition (i) guarantees that the dark state is $|1\rangle$ at the beginning and $|2\rangle$ at the end of the protocol. Condition (ii) implies that the eigenstate of the inertial Hamiltonian coincides with the dark state at t=0 and $t=t_f$. Finally, condition (iii) constrains the magnitude of the acceleration, minimizing non-adiabatic transitions in the inertial frame. In contrast to adiabatic conditions, the slope of θ during the protocol does not need to be small. This property enables, in principle, finding faster-than adiabatic solutions. The derivation of these conditions is given below.

To simplify the equations, we present the derivation in the limit of large detuning, although the result holds in general [9]. In this limit, the

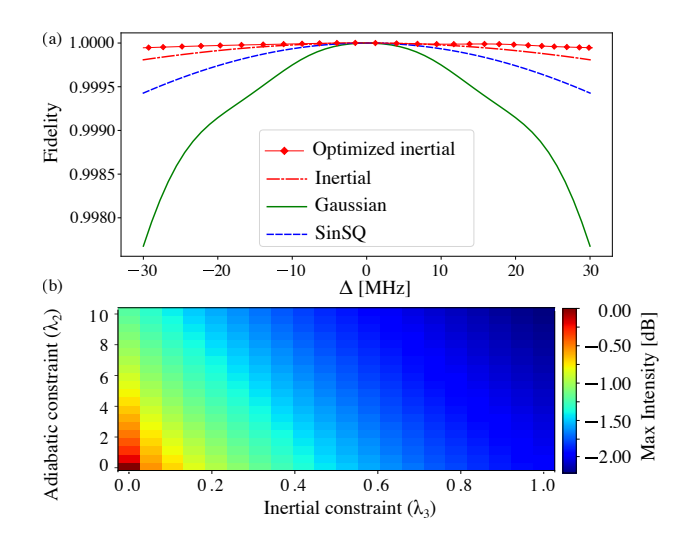


Fig. 3: Robust and efficient STIRAP solutions. (a) Robustness of the four protocols versus single-photon detuning Δ . (b) We perform QOCT and update the control fields using Eq. (13). Increasing the weights of adiabatic and inertial constraints, λ_2 and λ_3 , our algorithm finds solutions that reach fidelity of F=0.99 during $1\mu s$ with reduced pulse energy.

excited-state dynamics can be eliminated and the evolution in the ground-state manifold is governed by the Hamiltonian

$$H = \begin{pmatrix} \frac{\Omega_2^2 - \Omega_1^2}{2\Delta} & \frac{\Omega_2 \Omega_1}{\Delta} \\ \frac{\Omega_2 \Omega_1}{\Delta} & \frac{\Omega_1^2 - \Omega_2^2}{2\Delta} \end{pmatrix}. \tag{8}$$

(see Appendix A.) Substituting Eq. (6) into Eq. (8), one can rewrite the Hamiltonian in the form

$$H = \frac{\Omega^2}{2\Delta} \left(\cos 2\theta \sigma_z + \sin 2\theta \sigma_x \right). \tag{9}$$

Seeking an inertial solution, we transform the Hamiltonian to the eigenvector basis and find

$$\tilde{H} = \frac{\Omega^2}{2\Delta} \left(\sigma_z - \frac{\chi}{2} \sigma_y \right) = f(t) \mathbb{M}(\chi) \quad , \quad \chi \equiv \frac{\Delta \dot{\theta}}{\Omega^2}$$
(10)

with dot denoting a time derivative (see appendix B). The inertial protocol succeeds provided that $\mathbb{M}(\chi)$ varies slowly [condition (iii)] and that the eigenstates of $\mathbb{M}(\chi)$ and H coincide at the beginning and end of the protocol [condition (ii), because given this condition, both matrices are diagonal]. We considered Hamiltonian dynamics, but the same conditions apply to open systems (proven using Liouville space formalism presented in [9]).

In Fig. 2(c), we compare three analytic pulse shapes: Gaussian (solid green), squared sinusoidal (dashed blue), and "inertial" (dash-dot

red), with $\theta(t)$ satisfying conditions (i)–(iii) above. The pulses are defined as

Gaussian:
$$\Omega_{1,2}(t) = Ae^{-(t-t_i)^2/\sigma^2}$$
 (11a)

SinSQ:
$$\Omega_{1,2}(t) = A \sin^2[\pi(t - t_i)/2\tau]$$
 (11b)

Inertial: Use Eq. (6) with
$$\theta(t) = \sum_{i=0}^{3} C_i t^i$$
. (11c)

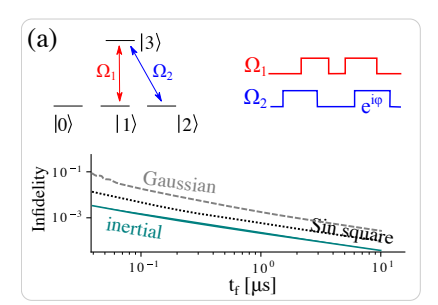
The Gaussian width is $\sigma = t_f/2$ and the peaks of the pulses are separated by t_f . The squared-sine pulse parameter is $\tau = t_f$, and the inertial coefficients are: $C_0 = C_1 = 0, C_2 = (\pi/2 - C_3 t_f^3)/tf^2$ and $C_3 = -\pi/t_f^3$. In Fig. 2(d), we compare their infidelity as a function of protocol duration. The infidelity, $1 - \text{Tr}\sqrt{\sqrt{\rho_f}\rho_t\sqrt{\rho_f}}$, is defined in terms of the overlap between the desired target, ρ_t , and final state, ρ_f . The infidelity of the protocols decreases upon increasing protocol duration. Small oscillations in the infidelity are observed in all three plots. These arise from non-adiabatic transitions that can be controlled by using mask functions that smooth the derivatives of the pulses, as explained in [31]. We find that the inertial protocol outperforms the other protocols. We improve these results further with optimization (red triangles). To this end, we perform an iterative algorithm, where we update the control fields in each step so that the target state is approached while minimizing non-adiabatic and non-inertial transitions.

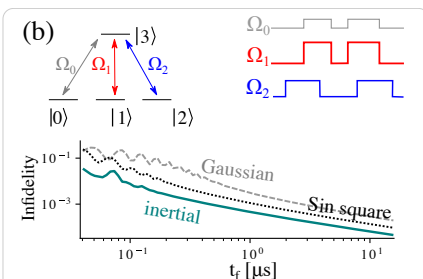
4 Optimal control with adiabatic inertial constraints

We construct a functional \mathcal{J} , whose minimal solution is an optimal inertial STIRAP solution. Consider the functional

$$\mathcal{J}(\rho,\Omega) = \text{Tr}\{\rho_t \rho_f\} - \int_0^{t_f} dt \, \text{Tr}\{\xi(t) \left[\frac{d}{dt} - \hat{\mathcal{L}}\right] \rho(t)\}$$
$$+ \lambda_1 \int_0^{t_f} dt |\Omega(t)|^2 + \lambda_2 \int_0^{t_f} dt |\dot{\Omega}(t)|^2 + \lambda_3 \int_0^{t_f} dt |\ddot{\Omega}(t)|^2$$
(12)

The quantum state is represented by a density matrix, ρ , and we use the symbol Ω to represent control fields (e.g., $\Omega_{1,2}$ in STIRAP). The first term is maximized when the system reaches the target state; that is, when $\rho_f = \rho_t$. The second enforces solutions to satisfy the Lindblad equation, $\dot{\rho} = \hat{\mathcal{L}}\rho$, where $\hat{\mathcal{L}}$ is the Lindbladian





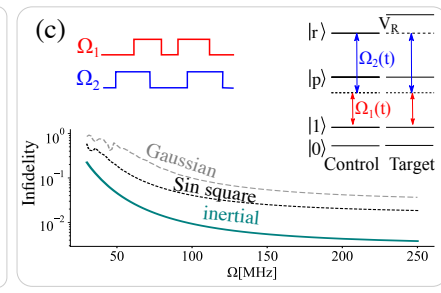


Fig. 4: Inertial geometric gates (a) Single-qubit phase gate, implemented using tripod-level atoms and two fields performing two STIRAP steps (top). Gate infidelity versus protocol duration for the three protocols (bottom). (b) Hadamard gate, implemented with three fields using two STIRAPs (top) and gate infidelity (bottom). (c) Controlled phase gate, based on two STIRAP steps and Rydberg-induced phase shifts (top) and gate infidelity versus maximal Rabi frequency (bottom).

operator, ξ is the associated Lagrange multiplier. The third term restricts the amount of power in the control pulses. We include the last two terms to restrict the time-averaged velocity and acceleration (in STIRAP, $\dot{\theta}$ and $\ddot{\theta}$ respectively). We use Krotov's method to optimize \mathcal{J} [32, 33, 34, 35, 36, 37], modified to include adiabatic and inertiality constraints. The algorithm starts from an initial guess for the controls, Ω , solves the equations of motion for ρ and ξ , and updates the guess, $\Omega \to \Omega + \Delta \Omega$, to decrease $\Delta \mathcal{J}$ in each iteration. The equations of motion for ρ and ξ are the Lindblad equation and its conjugate. The update equation for Ω (required to decrease \mathcal{J}) is

$$2\lambda_{1}\Delta\Omega_{R} - 2\lambda_{2}\Delta\ddot{\Omega}_{R} + 2\lambda_{3}\Delta\ddot{\Omega}_{R} = \operatorname{Tr}\{\xi^{k}\frac{\partial\Delta\hat{\mathcal{L}}}{\partial\Delta\Omega_{R}}\rho^{k+1}\}$$
$$2\lambda_{1}\Delta\Omega_{I} - 2\lambda_{2}\Delta\ddot{\Omega}_{I} + 2\lambda_{3}\Delta\ddot{\Omega}_{I} = \operatorname{Tr}\{\xi^{k}\frac{\partial\Delta\hat{\mathcal{L}}}{\partial\Delta\Omega_{I}}\rho^{k+1}\}.$$
(13)

Here $\Delta\Omega_R$ and $\Delta\Omega_I$ are the update rules of the real and imaginary parts of each control field in the k+1 iteration. The second and third terms on the left-hand side of Eq. (13) arise due to inertial and adiabatic constraints. These correspond to second- and fourth-order temporal derivatives. A complete derivation of the update equations is given in Appendix C, along with an alternative approach to impose the constraints (by maximizing the state projection onto the adiabatic or inertial subspaces).

We use Eq. (13) to find an optimal solution. Its fidelity is compared with unoptimized protocols in Fig. 2(d) and their robustness is shown in Fig. 3(a), demonstrating that the optimal protocol is highly robust with respect to variations in the single-photon detuning, Δ . Figure 3(b)

shows that when increasing the weight of the inertial constraint relative to the adiabatic constraint (e.g., taking $\lambda_3/\lambda_2 = 10$), one obtains a 2dB reduction in pulse energy for the same protocol duration. Having found optimal inertial and adiabatic solutions, we use those solutions to perform high-fidelity quantum logic gates.

5 Geometric quantum logic gates.

Adiabatic protocols have many applications in quantum information science. An important class of protocols involves cyclic evolution (which starts and ends with the same Hamiltonian) under which a qubit's state acquires a geometric phase that depends only on its path in the Hilbert While non-degenerate Hamiltonians are associated with scalar (abelian) phases, degeneracy gives rise to matrix (non-abelian) phases [39]. When including both abelian and non-abelian "holonomic" operations, it is possible to realize a universal set of gates that are robust against certain types of errors [40, 41, 42, 43, 44]. A protocol for holonomic quantum logic gates was proposed in [8], where the qubit state acquires geometric phases by driving transitions out and back into the qubit subspace. Such transitions can be driven using STIRAP. In this section, we apply our optimized pulses to implement these gates.

Let us review the principle of operation of the gates. Consider the tripod-level scheme shown in Fig. 4(a). The qubit state is encoded in the levels $|0\rangle$ and $|1\rangle$. To implement a phase gate, one uses two fields, Ω_1 and Ω_2 , to transfer population from $|1\rangle$ to the auxiliary level $|2\rangle$ and back into $|1\rangle$, using two STIRAP steps, as shown in the right in-

set. A phase gate is implemented by shifting the phase of Ω_2 in the second STIRAP step, which leads to an accumulated phase of the dark state. To implement a Hadamard gate [Fig. 4(b)], one needs a third field, Ω_0 . The three fields, $\Omega_{0,1,2}$, are applied following the protocol in the right inset. In this case, the dark state is a combination of $|0\rangle$ and $|1\rangle$, whose weights are determined by the ratio of Ω_0 and Ω_1 . During the protocol, a phase is acquired by the dark state, which translates into a rotation in the qubit basis [8, 28]. Finally, a controlled-phase gate is achieved using Rydberg interaction between excited states [Fig. 4(c)]. This gate operates in a regime of a weak Rydberg interaction compared to the Rabi frequencies, $V_R \ll \Omega_1, \Omega_2$. In this limit, when two atoms occupy the excited state, their interaction produces an energy shift and the wavefunction acquires a phase proportional to V_R . A controlled phase gate is implemented by applying two STIRAP steps (right inset) and tuning the time delay between the pulses such that the $|11\rangle$ component of the wavefunction acquires a phase of π .

We simulated these protocols using the three pulse shapes from Fig. 2. For each protocol, we reconstructed the simulated gate, $\rho \to \hat{G}(\rho)$, with process tomography (appendix E), which provides the Kraus operators, G_k , that can be used to write $\hat{\mathcal{G}}$ as: [45]

$$\hat{\mathcal{G}}(\rho) = \sum_{k} G_k \rho G_k^{\dagger}. \tag{14}$$

Using this expansion, we computed the average gate fidelity, \mathcal{F} , defined as the overlap between the simulated and target gates ($\hat{\mathcal{G}}$ and U_0 respectively) averaged over all possible initial states. For an initial pure state, $|\psi\rangle$, the average gate fidelity \mathcal{F} is given by [46, 47, 48, 49]:

$$\mathcal{F} \equiv \int_{S^{2n-1}} dV \left\langle \psi \left| U_0^{\dagger} \hat{G}(|\psi\rangle \langle \psi|) U_0 \right| \psi \right\rangle = \frac{1}{n(n+1)} \sum_{k} \left(\text{Tr}(M_k M_k^{\dagger}) + \left| \text{Tr}(M_k) \right|^2 \right), \quad (15)$$

where n is the dimension of the Hilbert space (2 for single-qubit gates and 4 for 2-qubit gates) and $M_k \equiv U_0^{\dagger} G_k$.

The results are shown in the bottom plots. For single-qubit gates, we plot the infidelity as a function of protocol duration, where the limit of large t_f corresponds to the adiabatic limit. For the

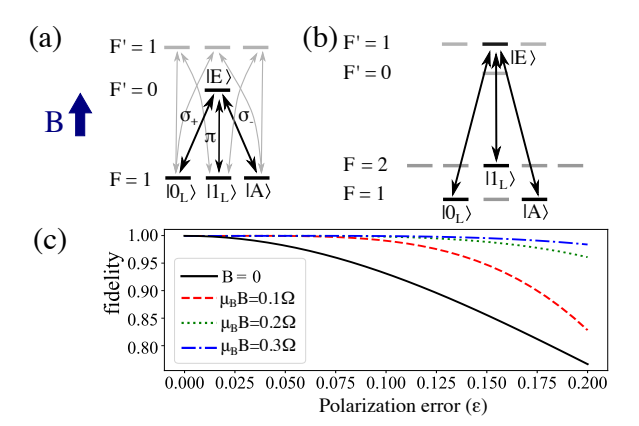


Fig. 5: **Inertial STIRAP protocol.** (a,b) Two possible realizations of a tripod level system using the D2 line of ⁸⁷Rb. Desired transitions (solid lines) are shown with the corresponding polarizations: circular (σ_{\pm}) and π . Additional transitions are shown by grey arrows. (c) Infidelity of the phase gate [Fig. 3(a)] versus polarization error, ε , defined as the fraction of undesired polarization in each STIRAP pulse.

controlled-phase gate, we plot the infidelity versus Rabi frequency, since t_f is set by requiring that the conditional phase shift is π . The inertial protocol approaches $\mathcal{F}=1$ at the fastest rate, as expected based on Fig. 2. Unfortunately, the gate fidelity is much smaller than the STI-RAP fidelity. The reason is that gate fidelities are limited by phase errors, which are larger than population errors that limit STIRAP ¹.

6 Experimental realization.

We analyze a realization of our protocol using ⁸⁷Rb atoms. Two possible choices of energy levels and transitions from the D2 line are shown in Fig. 5(a-b). In particular, we are interested in analyzing realistic imperfections, including polarization and leakage errors (following the analysis from [50, 51, 52, 53]). For example, consider a single-qubit phase gate implemented using the levels shown in Fig. 5(a). Ideally, to drive STIRAP transitions from the state $|0_L\rangle$ to $|A\rangle$ and back, we want to apply only two beams: The pulse Ω_1 with σ_+ polarization, which drives $|F=1,m_F=-1\rangle \leftrightarrow |F'=0,m_F=0\rangle$, and the pulse Ω_2 with σ_- polarization, which drives $|F=1,m_F=1\rangle \leftrightarrow |F'=0,m_F=0\rangle$. However,

¹It is a consequence of first-order perturbation theory that population errors scale quadratically with the small parameter while phase errors scale linearly.

polarization errors in the second pulse, Ω_2 , produce a σ_{+} component that drives the first transition, and errors in the first pulse drive the second transition. This process reduces the success probability of the protocol. To combat this issue, one can apply a DC magnetic field to shift the energy levels and tune the frequencies of the control fields to be in resonance with the shifted levels. By off-setting the frequencies of the Ω_1 and Ω_2 pulses, the error fields become off resonant and their effect is suppressed. Our calculation assumes that the magnetic field is in the weak Zeeman regime. A more accurate treatment should include nonlinear (Paschen-Back) corrections for fields exceeding 10G ². Our simulations demonstrate that the fidelity approaches unity when increasing the magnetic field [Fig. 5(c)].

7 Conclusion

In this work, we presented inertial protocols for STIRAP and geometric single- and two-qubit gates. We estimated the fidelity and robustness of our protocols using realistic experimental parameters, taking account of practical considerations including polarization impurity, spontaneous emission, and populating leakage (i.e., transitions out of the tripod system). We used a DC magnetic field to suppress polarization errors. The fidelity could be improved further by introducing a resonant optical cavity to enhance desired transitions, e.g., using the setup of [53]. In light of the long list of existing "improved adiabatic protocols," our work adds simple analytic pulse shapes that yield nearly optimal solutions by satisfying the condition of small acceleration [9]. Another strength of our approach is that we consider Lindbladian dynamics in the optimization process, so the various decay channels with their respective branching ratios affect the optimal solution. Indeed, we find in some cases optimal pulses with two humps, as opposed to standard quasi-Gaussian pulses. A downside of our approach is that our protocols are not robust to perturbations in the geometric phase acquired during the protocol, but are rather determined by it. It would be intriguing to optimize adiabatic protocols that are topologically robust

 $^2 Field$ stength of 10G corresponds to the green curve at Rabi frequency $\Omega = 50 MHz.$

to errors (such as [54, 55]) in future work. Finally, we note that the presented inertial solutions are also adiabatic in the sense that the control fields do not vary rapidly in comparison to the energy gap. The reason is that when considering protocols that satisfy the conditions of Eq. (7), strong violations of adiabaticity imply violations of inertiality. We hypothesize that inertial non-adiabatic solutions exist in other cases. To conclude, due to immense recent progress in quantum computation research and the ability to prepare and manipulate large registers of atomic qubits [56, 57, 3], our protocols are directly applicable and could be used to improve gate fidelities in these platforms.

Acknowledgement

The authors would like to thank Aviv Aroch for helping us set up and run Krotov's algorithm. A.P. acknowledges support from the Alon Fellowship of the Israeli Council of Higher Education. B.D. acknowledges support from the Israeli Science Foundation, the Binational Science Foundation, H2020 Excellent Science (DAALI, 899275), the Minerva Foundation. R.K. acknowledges support from the Israeli Science Foundation, grant number 526/21. R.D. acknowledges support from the Adams Fellowship Program of the Israel Academy of Science and Humanities.

References

- [1] T. D. Ladd, F. Jelezko, R. Laflamme, Y. Nakamura, C. Monroe, and J. L. O'Brien, "Quantum computers," nature, vol. 464, no. 7285, pp. 45–53, 2010.
- [2] M. Saffman, "Quantum computing with atomic qubits and rydberg interactions: progress and challenges," Journal of Physics B: Atomic, Molecular and Optical Physics, vol. 49, no. 20, p. 202001, 2016.
- [3] L. Henriet, L. Beguin, A. Signoles, T. Lahaye, A. Browaeys, G.-O. Reymond, and C. Jurczak, "Quantum computing with neutral atoms," *Quantum*, vol. 4, p. 327, 2020.
- [4] M. Morgado and S. Whitlock, "Quantum simulation and computing with rydberg-interacting qubits," AVS Quantum Science, vol. 3, no. 2, p. 023501, 2021.

- [5] C. Zhang, F. Pokorny, W. Li, G. Higgins, A. Pöschl, I. Lesanovsky, and M. Hennrich, "Submicrosecond entangling gate between trapped ions via rydberg interaction," *Nature*, vol. 580, no. 7803, pp. 345–349, 2020.
- [6] D. Aharonov and M. Ben-Or, "Fault-tolerant quantum computation with constant error," in *Proceedings of the twenty-ninth annual ACM symposium on Theory of computing*, pp. 176–188, 1997.
- [7] N. V. Vitanov, A. A. Rangelov, B. W. Shore, and K. Bergmann, "Stimulated raman adiabatic passage in physics, chemistry, and beyond," *Reviews of Modern Physics*, vol. 89, no. 1, p. 015006, 2017.
- [8] D. Møller, L. B. Madsen, and K. Mølmer, "Geometric phase gates based on stimulated raman adiabatic passage in tripod systems," *Physical Review A*, vol. 75, no. 6, p. 062302, 2007.
- [9] R. Dann and R. Kosloff, "Inertial theorem: Overcoming the quantum adiabatic limit," *Physical Review Research*, vol. 3, no. 1, p. 013064, 2021.
- [10] C.-K. Hu, R. Dann, J.-M. Cui, Y.-F. Huang, C.-F. Li, G.-C. Guo, A. C. Santos, and R. Kosloff, "Experimental verification of the inertial theorem control protocols," *New Journal of Physics*, vol. 23, no. 9, p. 093048, 2021.
- [11] D. Sels and A. Polkovnikov, "Minimizing irreversible losses in quantum systems by local counterdiabatic driving," *Proceedings of the National Academy of Sciences*, vol. 114, no. 20, pp. E3909–E3916, 2017.
- [12] M. V. Berry, "Transitionless quantum driving," Journal of Physics A: Mathematical and Theoretical, vol. 42, no. 36, p. 365303, 2009.
- [13] R. Unanyan, L. Yatsenko, K. Bergmann, and B. Shore, "Laser-induced adiabatic atomic reorientation with control of diabatic losses," *Optics communications*, vol. 139, no. 1-3, pp. 48–54, 1997.
- [14] M. Demirplak and S. A. Rice, "Adiabatic population transfer with control fields," *The Journal of Physical Chemistry A*, vol. 107, no. 46, pp. 9937–9945, 2003.

- [15] X. Chen, I. Lizuain, A. Ruschhaupt, D. Guéry-Odelin, and J. Muga, "Shortcut to adiabatic passage in two-and three-level atoms," *Physical review letters*, vol. 105, no. 12, p. 123003, 2010.
- [16] E. Torrontegui, S. Ibáñez, S. Martínez-Garaot, M. Modugno, A. del Campo, D. Guéry-Odelin, A. Ruschhaupt, X. Chen, and J. G. Muga, "Shortcuts to adiabaticity," in *Advances in atomic, molecular, and optical physics*, vol. 62, pp. 117–169, Elsevier, 2013.
- [17] A. del Campo, "Shortcuts to adiabaticity by counterdiabatic driving," *Physical review letters*, vol. 111, no. 10, p. 100502, 2013.
- [18] D. Guéry-Odelin, A. Ruschhaupt, A. Kiely, E. Torrontegui, S. Martínez-Garaot, and J. G. Muga, "Shortcuts to adiabaticity: Concepts, methods, and applications," *Reviews of Modern Physics*, vol. 91, no. 4, p. 045001, 2019.
- [19] A. Benseny and K. Mølmer, "Adiabatic theorem revisited: The unexpectedly good performance of adiabatic passage," *Physical Review A*, vol. 103, no. 6, p. 062215, 2021.
- [20] Y.-X. Du, Z.-T. Liang, Y.-C. Li, X.-X. Yue, Q.-X. Lv, W. Huang, X. Chen, H. Yan, and S.-L. Zhu, "Experimental realization of stimulated raman shortcut-to-adiabatic passage with cold atoms," *Nature communications*, vol. 7, no. 1, p. 12479, 2016.
- [21] G. Vasilev, A. Kuhn, and N. Vitanov, "Optimum pulse shapes for stimulated raman adiabatic passage," *Physical Review A*, vol. 80, no. 1, p. 013417, 2009.
- [22] X. Chen and J. Muga, "Engineering of fast population transfer in three-level systems," *Physical Review A*, vol. 86, no. 3, p. 033405, 2012.
- [23] V. S. Malinovsky and D. J. Tannor, "Simple and robust extension of the stimulated raman adiabatic passage technique to n-level systems," *Physical Review A*, vol. 56, no. 6, p. 4929, 1997.
- [24] J. Werschnik and E. Gross, "Quantum optimal control theory," *Journal of Physics B: Atomic, Molecular and Optical Physics*, vol. 40, no. 18, p. R175, 2007.

- [25] C. P. Koch, U. Boscain, T. Calarco, G. Dirr, S. Filipp, S. J. Glaser, R. Kosloff, S. Montangero, T. Schulte-Herbrüggen, D. Sugny, et al., "Quantum optimal control in quantum technologies. strategic report on current status, visions and goals for research in europe," EPJ Quantum Technology, vol. 9, no. 1, p. 19, 2022.
- [26] R. Unanyan, B. Shore, and K. Bergmann, "Laser-driven population transfer in fourlevel atoms: Consequences of non-abelian geometrical adiabatic phase factors," *Physi*cal Review A, vol. 59, no. 4, p. 2910, 1999.
- [27] L.-M. Duan, J. I. Cirac, and P. Zoller, "Geometric manipulation of trapped ions for quantum computation," *Science*, vol. 292, no. 5522, pp. 1695–1697, 2001.
- [28] K. Toyoda, K. Uchida, A. Noguchi, S. Haze, and S. Urabe, "Realization of holonomic single-qubit operations," *Physical Review A*, vol. 87, no. 5, p. 052307, 2013.
- [29] X. Lacour, N. Sangouard, S. Guerin, and H.-R. Jauslin, "Arbitrary state controlledunitary gate by adiabatic passage," *Physical Review A*, vol. 73, no. 4, p. 042321, 2006.
- [30] D. Daems and S. Guerin, "Analog grover search by adiabatic passage in a cavity-laser-atom system," *Physical Review A*, vol. 78, no. 2, p. 022330, 2008.
- [31] T. A. Laine and S. Stenholm, "Adiabatic processes in three-level systems," *Physical Review A*, vol. 53, no. 4, p. 2501, 1996.
- [32] V. F. Krotov and I. Feldman, "An iterative method for solving optimal-control problems," *Engineering cybernetics*, vol. 21, no. 2, pp. 123–130, 1983.
- [33] A. Bartana, R. Kosloff, and D. J. Tannor, "Laser cooling of internal degrees of freedom. ii," *The Journal of chemical physics*, vol. 106, no. 4, pp. 1435–1448, 1997.
- [34] D. J. Tannor, V. Kazakov, and V. Orlov, "Control of photochemical branching: Novel procedures for finding optimal pulses and global upper bounds," *Time-dependent quantum molecular dynamics*, pp. 347–360, 1992.
- [35] V. F. Krotov, "A technique of global bounds in optimal control theory," Control and Cybernetics, vol. 17, no. 3, pp. 2–3, 1988.

- [36] V. Krotov, Global methods in optimal control theory, vol. 195. CRC Press, 1995.
- [37] A. Konnov and V. F. Krotov, "On global methods of successive improvement of controlled processes," *Automation and Remote* Control, vol. 60, no. 10, pp. 1427–1436, 1999.
- [38] T. Kato, "On the adiabatic theorem of quantum mechanics," *Journal of the Physical Society of Japan*, vol. 5, no. 6, pp. 435–439, 1950.
- [39] P. Zanardi and M. Rasetti, "Holonomic quantum computation," *Physics Letters A*, vol. 264, no. 2-3, pp. 94–99, 1999.
- [40] M. Saffman and K. Mølmer, "Efficient multiparticle entanglement via asymmetric rydberg blockade," *Physical review letters*, vol. 102, no. 24, p. 240502, 2009.
- [41] D. B. Rao and K. Mølmer, "Dark entangled steady states of interacting rydberg atoms," *Physical review letters*, vol. 111, no. 3, p. 033606, 2013.
- [42] D. B. Rao and K. Mølmer, "Deterministic entanglement of rydberg ensembles by engineered dissipation," *Physical Review A*, vol. 90, no. 6, p. 062319, 2014.
- [43] D. Petrosyan, F. Motzoi, M. Saffman, and K. Mølmer, "High-fidelity rydberg quantum gate via a two-atom dark state," *Physical Review A*, vol. 96, no. 4, p. 042306, 2017.
- [44] M. Khazali and K. Mølmer, "Fast multiqubit gates by adiabatic evolution in interacting excited-state manifolds of rydberg atoms and superconducting circuits," *Physical Review X*, vol. 10, no. 2, p. 021054, 2020.
- [45] M. A. Nielsen and I. Chuang, "Quantum computation and quantum information," 2002.
- [46] M. A. Nielsen, "A simple formula for the average gate fidelity of a quantum dynamical operation," *Physics Letters A*, vol. 303, no. 4, pp. 249–252, 2002.
- [47] I. Beterov, M. Saffman, E. Yakshina, D. Tretyakov, V. Entin, G. Hamzina, and I. Ryabtsev, "Simulated quantum process tomography of quantum gates with rydberg superatoms," *Journal of Physics B: Atomic, Molecular and Optical Physics*, vol. 49, no. 11, p. 114007, 2016.

- [48] M. H. Goerz, E. J. Halperin, J. M. Aytac, C. P. Koch, and K. B. Whaley, "Robustness of high-fidelity rydberg gates with single-site addressability," *Physical Review A*, vol. 90, no. 3, p. 032329, 2014.
- [49] L. H. Pedersen, N. M. Møller, and K. Mølmer, "Fidelity of quantum operations," *Physics Letters A*, vol. 367, no. 1-2, pp. 47–51, 2007.
- [50] I. Shomroni, S. Rosenblum, Y. Lovsky, O. Bechler, G. Guendelman, and B. Dayan, "All-optical routing of single photons by a one-atom switch controlled by a single photon," *Science*, vol. 345, no. 6199, pp. 903– 906, 2014.
- [51] S. Rosenblum, O. Bechler, I. Shomroni, Y. Lovsky, G. Guendelman, and B. Dayan, "Extraction of a single photon from an optical pulse," *Nature Photonics*, vol. 10, no. 1, pp. 19–22, 2016.
- [52] S. Rosenblum, A. Borne, and B. Dayan, "Analysis of deterministic swapping of photonic and atomic states through single-photon raman interaction," *Physical Review A*, vol. 95, no. 3, p. 033814, 2017.
- [53] O. Bechler, A. Borne, S. Rosenblum, G. Guendelman, O. E. Mor, M. Netser, T. Ohana, Z. Aqua, N. Drucker, R. Finkelstein, et al., "A passive photon—atom qubit swap operation," Nature Physics, vol. 14, no. 10, pp. 996–1000, 2018.
- [54] A. Kitaev and C. Laumann, "Topological phases and quantum computation," Exact methods in low-dimensional statistical physics and quantum computing, pp. 101–125, 2010.
- [55] V. Lahtinen and J. Pachos, "A short introduction to topological quantum computation," *SciPost Physics*, vol. 3, no. 3, p. 021, 2017.
- [56] D. Barredo, S. De Léséleuc, V. Lienhard, T. Lahaye, and A. Browaeys, "An atomby-atom assembler of defect-free arbitrary two-dimensional atomic arrays," *Science*, vol. 354, no. 6315, pp. 1021–1023, 2016.
- [57] H. Bernien, S. Schwartz, A. Keesling, H. Levine, A. Omran, H. Pichler, S. Choi, A. S. Zibrov, M. Endres, M. Greiner, et al.,

"Probing many-body dynamics on a 51-atom quantum simulator," *Nature*, vol. 551, no. 7682, pp. 579–584, 2017.

Supplementary Information

A. Effective 2-level Hamiltonian for STIRAP

In this appendix, we present a Derivation of Eq. (6) from the main text. Consider the Hamiltonian of a 3-level system from driven by two optical fields (as shown in Fig. 2):

$$H = \Omega_1 |1\rangle\langle 3| + \Omega_2 |1\rangle\langle 2| + h.c. + \Delta |3\rangle\langle 3|. \tag{16}$$

Let us express the wavefunction as

$$|\psi\rangle = c_1|1\rangle + c_2|2\rangle + c_3|3\rangle. \tag{17}$$

We substitute this expansion into the Schrödinger equation $i\hbar \frac{d|\psi\rangle}{dt} = H|\psi\rangle$, to obtain the equations of motion for the coefficients:

$$i\hbar \dot{c}_1 = \Omega_1 c_3$$

$$i\hbar \dot{c}_2 = \Omega_2 c_3$$

$$i\hbar \dot{c}_3 = \Omega_1^* c_1 + \Omega_2^* c_2 + \Delta c_3.$$
(18)

In the limit of large detuning, $\Delta \gg \Omega_1, \Omega_2$, on can adiabatically eliminate the dynamics of the third level, setting $\dot{c}_3 = 0$. This assumption yields the relation

$$c_3 = -\frac{\Omega_1^*}{\Delta}c_1 - \frac{\Omega_2^*}{\Delta}c_2. \tag{19}$$

Substituting Eq. (19) into Eq. (18), we obtain

$$i\hbar\dot{c}_1 = -\frac{|\Omega_1|^2}{\Delta}c_1 - \frac{\Omega_1\Omega_2^*}{\Delta}c_2$$

$$i\hbar\dot{c}_2 = -\frac{|\Omega_2|^2}{\Delta}c_2 - \frac{\Omega_2\Omega_1^*}{\Delta}c_1$$
(20)

The dynamics is described by the effective Hamiltonian

$$H = \begin{pmatrix} \frac{|\Omega_1|^2}{2\Delta} & \frac{\Omega_2^*\Omega_1}{\Delta} \\ \frac{\Omega_2\Omega_1^*}{\Delta} & \frac{|\Omega_2|^2}{2\Delta} \end{pmatrix}. \tag{21}$$

By subtracting a constant-diagonal matrix, $\frac{|\Omega_1|^1 - |\Omega_2|^2}{2\Delta} \cdot \mathcal{I}$, from Eq. (21) one obtains Eq. (6). Subtracting a constant diagonal matrix only shifts the energy spectrum by a constant, symmetrizing it around zero, without affecting the dynamics otherwise.

B. Inertial STIRAP Hamiltonian

In this section, we derive Eq. (9) from the main text. We choose the parameterization

$$\Omega_1 = \Omega \sin \theta \quad , \quad \Omega_2 = \Omega \cos \theta.$$
(22)

The 2-level Hamiltonian [Eq. (6) from the main text] becomes

$$H = \frac{\Omega^2}{2\Lambda} \left(\cos 2\theta \sigma_z + \sin 2\theta \sigma_x\right) \tag{23}$$

where σ_x and σ_z are Pauli matrices. We obtain an explicit expression for the inertial-frame Hamiltonian defined as

$$\tilde{H} \equiv P^{\dagger} H P - i\hbar P^{\dagger} \frac{\partial P}{\partial t} \tag{24}$$

The eigenvalues are $\pm\Omega$. The eigenvector matrix is

$$P = \begin{pmatrix} \frac{\cot 2\theta + \csc 2\theta}{\sqrt{\cot \theta^2 + 1}} & \frac{\cot 2\theta - \csc 2\theta}{\sqrt{\tan \theta^2 + 1}} \\ \frac{1}{\sqrt{\cot \theta^2 + 1}} & \frac{1}{\sqrt{\tan \theta^2 + 1}} \end{pmatrix}. \tag{25}$$

For $0 < \theta < \pi$, we find

$$P^{\dagger} \frac{dP}{d\theta} = \frac{\dot{\theta}}{2} \begin{pmatrix} 0 & -1 \\ 1 & 0 \end{pmatrix}.$$

This completes the proof of Eq. (9) in the main text.

One finds a striking similarity between the inertial-frame Hamiltonian, Eq. (9), and the Hamiltonian one obtains when adding counter-diabatic terms to the lab-frame Hamiltonian realizing the shortcut-to-adiabaticity protocol (see Eqs. (4-5) in the Methods section of [20]). The similarity is expected, since the inner product of the instantaneous eigenvectors and their derivatives appear in both formulations. However, there is a conceptual difference which is important to point out. In shortcut-to-adiabaticity, one constructs a Hamiltonian, which may be challenging to realize, but whose eigenstates are exact solutions to the dynamics. In contrast, in our approach, the lab-frame Hamiltonian is straightforward, and the instantaneous eigenstates of the inertial-frame solutions are only approximations to the true dynamics.

C. Adiabatic and inertial constraints in QOCT

In this section, we generalize Krotov's QOCT algorithm to include inertial and adiabatic constrains. We present to approaches: in the first, we add a penalty for the time averaged velocity and acceleration, while in the second, we penalize instantaneous population in non-adiabatic and non-inertial states. We follow the derivation of [33] with appropriate modifications to our problem.

C1. Introducing penalty terms for the time-averaged velocity and acceleration

Let us consider the following functional to be minimized:

$$\mathcal{J} = \text{Tr}\{\rho_t \rho_f\} - \int_0^{t_f} dt \text{Tr}\{\xi(t) \left[\frac{d}{dt} - \hat{\mathcal{L}}\right] \rho(t)\}$$

$$+ \lambda_1 \int_0^{t_f} dt |\Omega(t)|^2 + \lambda_2 \int_0^{t_f} dt |\dot{\Omega}(t)|^2 + \lambda_3 \int_0^{t_f} dt |\ddot{\Omega}(t)|^2$$
(26)

where the two last terms correspond to the integrated velocity and acceleration. Using integration by parts, one can rewrite the first line of Eq. (26) as:

$$\operatorname{Tr}\left\{\rho_{t}\rho_{f}-(\xi\,\rho)|_{0}^{t_{f}}+\int_{0}^{t_{f}}dt\left[\rho\frac{d\xi}{dt}+\xi\hat{\mathcal{L}}\rho\right]\right\}.\tag{27}$$

Krotov's algorithm starts with an initial guess from the control fields, evolves ρ and ξ and finds an updated control pulse that decreases \mathcal{J} . By iteratively updating the control pulse, convergence is reached. Let us compute the change in \mathcal{J} between iteration k and k+1 in terms of the change in ρ . Using the definitions

$$\Delta \mathcal{J} = \mathcal{J}^{(k+1)} - \mathcal{J}^{(k)} \quad , \quad \Delta \rho = \rho^{(k+1)} - \rho^{(k)}, \tag{28}$$

we obtain:

$$\Delta \mathcal{J} = \operatorname{Tr} \left\{ \rho_t \Delta \rho - \xi^k \Delta \rho \right]_0^{t_f} \right\} +$$

$$\operatorname{Tr} \left\{ \int_0^{t_f} dt \left[\Delta \rho \frac{d\xi}{dt} + \xi^k \hat{\mathcal{L}} \Delta \rho + \xi^k \Delta \hat{\mathcal{L}} \rho^{(k+1)} \right] \right\} +$$

$$- \int_0^{t_f} \left\{ 2\lambda_1 \operatorname{Re} \left[\varepsilon^k \Delta \varepsilon^* \right] + \lambda_1 \left[\Delta \varepsilon_R^2 + \Delta \varepsilon_I^2 \right] \right\} +$$

$$- \int_0^{t_f} \left\{ 2\lambda_2 \operatorname{Re} \left[\dot{\varepsilon}^k \Delta \dot{\varepsilon}^* \right] + \lambda_2 \left[\Delta \dot{\varepsilon}_R^2 + \Delta \dot{\varepsilon}_I^2 \right] \right\} +$$

$$- \int_0^{t_f} \left\{ 2\lambda_3 \operatorname{Re} \left[\ddot{\varepsilon}^k \Delta \ddot{\varepsilon}^* \right] + \lambda_3 \left[\Delta \ddot{\varepsilon}_R^2 + \Delta \ddot{\varepsilon}_I^2 \right] \right\}. \tag{29}$$

The first 4 terms do not depend on the field increment and produce the dynamical equations for ρ and ξ . The additional terms produce the differential: $\Delta \mathcal{J}_1 + \Delta \mathcal{J}_2 + \Delta \mathcal{J}_3 + \Delta \mathcal{J}_4$ where

$$\Delta \mathcal{J}_{1} = \operatorname{Tr} \left\{ \int_{0}^{t_{f}} dt \xi^{k} \Delta \hat{\mathcal{L}} \rho^{(k+1)} \right\}$$

$$\Delta \mathcal{J}_{2} = -2\operatorname{Re} \left[\int_{0}^{t_{f}} \lambda_{1} \varepsilon^{k} \Delta \varepsilon^{*} + \lambda_{2} \dot{\varepsilon}^{k} \Delta \dot{\varepsilon}^{*} + \lambda_{3} \ddot{\varepsilon}^{k} \Delta \ddot{\varepsilon}^{*} \right]$$

$$\Delta \mathcal{J}_{3} = -\int_{0}^{t_{f}} \lambda_{1} \Delta \varepsilon_{R}^{2} + \lambda_{2} \Delta \dot{\varepsilon}_{R}^{2} + \lambda_{3} \Delta \ddot{\varepsilon}_{R}^{2}$$

$$\Delta \mathcal{J}_{4} = -\int_{0}^{t_{f}} \lambda_{1} \Delta \varepsilon_{I}^{2} + \lambda_{2} \Delta \dot{\varepsilon}_{I}^{2} + \lambda_{3} \Delta \ddot{\varepsilon}_{I}^{2}.$$
(30)

The term $\Delta \mathcal{J}_2$ vanishes on average since the integrand is rapidly oscillating. The complete differential of the third term is

$$d(\Delta \mathcal{J}_{3}) = \int_{0}^{t_{f}} df (\Delta \varepsilon_{R}, \Delta \dot{\varepsilon}_{R}, \Delta \ddot{\varepsilon}_{R}) dt =$$

$$\int_{0}^{t_{f}} \left[\frac{df}{d\Delta \varepsilon_{R}} \Delta \varepsilon_{R} + \frac{df}{d\Delta \dot{\varepsilon}_{R}} \Delta \dot{\varepsilon}_{R} + \frac{df}{d\Delta \ddot{\varepsilon}_{R}} \Delta \ddot{\varepsilon}_{R} \right] dt$$

$$\int_{0}^{t_{f}} \left[\frac{\partial f}{\partial \Delta \varepsilon_{R}} - \frac{d}{dt} \frac{\partial f}{\partial \Delta \dot{\varepsilon}_{R}} + \frac{d^{2}}{dt^{2}} \frac{\partial f}{\partial \Delta \ddot{\varepsilon}_{R}} \right] \Delta \varepsilon_{R} dt + \text{surface terms}$$

$$2 \int_{0}^{t_{f}} (-\lambda_{1} \Delta \varepsilon_{R} + \lambda_{2} \Delta \ddot{\varepsilon}_{R} - \lambda_{3} \Delta \ddot{\varepsilon}_{R}) + \text{surface terms}$$
(31)

The surface terms vanish since the field update at the start and end point is zero, $\Delta \varepsilon_R(0) = \Delta \varepsilon_R(t_f) = 0$. Using this result (and repeating the same procedure for $\Delta \mathcal{J}_4$), we find update equations:

$$-\lambda_1 \Delta \varepsilon_R + \lambda_2 \Delta \ddot{\varepsilon}_R - \lambda_3 \Delta \ddot{\varepsilon}_R = \frac{1}{2} \text{Tr} \left[\xi^k \frac{\partial \Delta \hat{\mathcal{L}}}{\partial \Delta \varepsilon_R} \rho^{k+1} \right] \equiv F(t)$$

$$-\lambda_1 \Delta \varepsilon_I + \lambda_2 \Delta \ddot{\varepsilon}_I - \lambda_3 \Delta \ddot{\varepsilon}_I = \frac{1}{2} \text{Tr} \left[\xi^k \frac{\partial \Delta \hat{\mathcal{L}}}{\partial \Delta \varepsilon_I} \rho^{k+1} \right] \equiv G(t)$$
(32)

These equations are easily solved by discretizing time and rewriting the equation in matrix form (the second-order time derivatives becomes the tridiagonal Hessian matrix and the fourth-order time derivatives is a 5-diagonal matrix). We obtain equations of the form

$$\mathbb{M}_1 \Delta \varepsilon_R = \mathbb{F}
\mathbb{M}_2 \Delta \varepsilon_I = \mathbb{G}$$
(33)

The update rules for the control fields are found by inverting M_1 and M_2 .

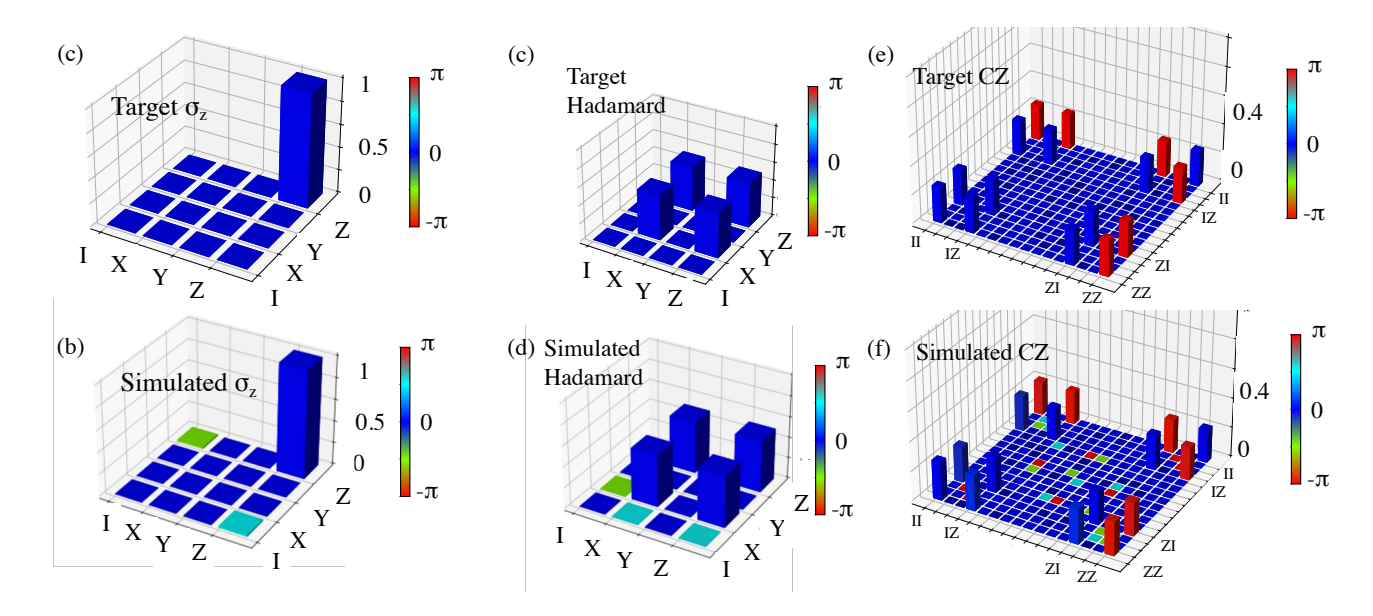


Fig. 6: **Quantum gate tomography:** Visualization of target (top) and simulated (bottom) single- and two-qubit gates. The plots show the matrix χ , which expresses the expansion coefficients of the gate transformations in terms of Pauli basis operators, \tilde{E}_i [Eq. (39)] for single-qubit gates and Kronecker products of \tilde{E}_i for two-qubit gates respectively. (a–d) The matrix χ , calculated using Eq. (41), for Hadamard and Pauli-Z single-qubit gates. (e,f) The matrix χ , calculated via Eq. (43) for a two-qubit controlled-phase gate.

C2. Maximize projection onto desired subspace

In this section, we present an alternative approach for optimization. We used both protocols in our simulations, choosing the protocol with the fastest convergence by trial and error. In this case, we impose adiabatic and inertial constraints by maximizing the projections onto adiabatic or inertial eigenstates. Denoting the projection operator by P (e.g., $P = |D\rangle \langle D|$ for adiabatic protocols), we penalize undesired transitions by introducing the last term in the functional

$$\mathcal{J} = \operatorname{Tr} \left\{ \rho_t \rho_f \right\} - \int_0^{t_f} dt \operatorname{Tr} \left\{ \xi(t) \left[\frac{d}{dt} - \hat{\mathcal{L}} \right] \rho(t) \right\}$$
$$+ \lambda_1 \int_0^{t_f} dt |\Omega(t)|^2 - \lambda_2 \int_0^{t_f} dt \operatorname{Tr} \left(P \rho \right) (P \rho)^{\dagger}$$
(34)

For convenience, we rewrite the integrand of the last term in the form

$$\operatorname{Tr}(P\rho)(P\rho)^{\dagger} = \operatorname{Tr}(P\rho)(\rho P) = \operatorname{Tr}\rho P\rho. \tag{35}$$

To derive optimization equations, we compute the full differential of \mathcal{J} with respect to $\delta\rho$, $\delta\xi$ and Ω . The new constraint modifies only terms related to $\delta\rho$. Specifically, taking the differential of Eq. (35) with respect to $\delta\rho$, we obtain Tr $(2P\rho)\delta\rho$. Revisiting all terms in Eq. (34), one can see that the second term also contributed to $\delta\rho$. After integration by parts, from the integral term in Eq. (27), we have

$$\frac{\partial \mathcal{J}}{\partial \rho} \delta \rho = \text{Tr} \int_0^{t_f} dt \left[\frac{d\xi}{dt} + \xi \hat{\mathcal{L}} + 2\lambda_2 P \rho \right] \delta \rho \tag{36}$$

We obtain a modified equation of motion for the Lagrange multiplier

$$\frac{d\xi}{dt} + \hat{\mathcal{L}}^{\dagger}\xi + 2\lambda_2 P\rho = 0 \tag{37}$$

The equation of motion of ρ and the update equation for the field are unaltered by the projection constraint. We obtain an equation of the Lindblad form with an inhomogeneous source term, which we can solve by standard numerical methods.

D. Quantum gate tomography

Quantum process tomography (QPT) is a method by which a quantum gate is reconstructed from simulated data (experimental or numerical). In this work, we use QPT to quantify the overlap between our simulated and target gates. In this appendix, we review the method presented in [45].

Suppose that a density matrix ρ evolves under our simulation into $\mathcal{G}(\rho)$. The goal of QPT is to determine \mathcal{G} . Given a complete basis of matrices, \tilde{E}_m , that spans the operator space (i.e., the Liouville space), any unitary \mathcal{G} can be written in the form

$$\mathcal{G}(\rho) = \sum_{m,n} \chi_{mn} \tilde{E}_m \rho \tilde{E}_n^{\dagger}, \tag{38}$$

where χ_{mn} are coefficients that we wish to find. For single-qubit gates, the set $\tilde{E_m}$ contains four 2×2 matrices (m = 1, ..., 4) and χ_{mn} is a 4×4 matrix. Let us choose the Pauli and identity matrices as basis operators:

$$\tilde{E}_1 = I$$
 , $\tilde{E}_2 = \sigma_x$, $\tilde{E}_3 = -i\sigma_y$, $\tilde{E}_4 = \sigma_z$. (39)

To determine χ , we run our simulations on 4 initial states

$$\rho_1 = |0\rangle\langle 0|, \ \rho_2 = \rho_1 \sigma_x, \ \rho_3 = \sigma_x \rho_1, \ \rho_4 = \sigma_x \rho_1 \sigma_x.$$
(40)

We compute the final state for every input: $\rho'_i \equiv \mathcal{E}(\rho_i)$. Then, following [45], χ is given by

$$\chi = \frac{1}{4} \begin{pmatrix} I & \sigma_x \\ \sigma_x & I \end{pmatrix} \begin{pmatrix} \rho_1' & \rho_2' \\ \rho_3' & \rho_4' \end{pmatrix} \begin{pmatrix} I & \sigma_x \\ \sigma_x & I \end{pmatrix}. \tag{41}$$

where $I, \sigma_x, \rho'_1, ..., \rho'_4 \in \mathbb{R}^{2 \times 2}$ and $\chi \in \mathbb{R}^{4 \times 4}$.

For two-qubit gates, we write

$$\mathcal{G}(\rho) = \sum_{m,n} \chi_{mn} \tilde{E}_m^{(2)} \rho(\tilde{E}_n^{(2)})^{\dagger}$$

$$\tag{42}$$

in terms of two-qubit operators, $\tilde{E}_m^{(2)} \in \mathbb{R}^{4\times 4}$, defined as Kronecker products of the single-qubit basis operators, \tilde{E}_m , from Eq. (39). The matrix $\chi \in \mathbb{R}^{16\times 16}$ is given by

$$\chi = \Lambda \,\bar{\rho} \,\Lambda,\tag{43}$$

where $\Lambda \in \mathbb{R}^{16 \times 16}$ is a rotation matrix

$$\Lambda \equiv \frac{1}{4} \left[\begin{pmatrix} I & \sigma_x \\ \sigma_x & I \end{pmatrix} \otimes \begin{pmatrix} I & \sigma_x \\ \sigma_x & I \end{pmatrix} \right] \tag{44}$$

and $\bar{\rho} \in \mathbb{R}^{16 \times 16}$ is defined as

$$\bar{\rho} = P^T \rho' P. \tag{45}$$

Here, $\rho' \in \mathbb{R}^{16 \times 16}$ the matrix of final states

$$\rho' = \mathcal{G}(\rho),\tag{46}$$

found by propagating 16 input states

$$\rho_{mn} = T_n |00\rangle \langle 00| T_m \quad \forall n, m = 1, ..., 4$$
(47)

with

$$T_1 = I \otimes I \quad , \quad T_2 = I \otimes \sigma_x$$

 $T_3 = \sigma_x \otimes I \quad , \quad T_4 = \sigma_x \otimes \sigma_x.$ (48)

The permutation matrix P is given by

$$P = I \otimes \begin{bmatrix} \begin{pmatrix} 1 & 0 & 0 & 0 \\ 0 & 0 & 1 & 0 \\ 0 & 1 & 0 & 0 \\ 0 & 0 & 0 & 1 \end{pmatrix} \otimes I \end{bmatrix}. \tag{49}$$

Note that $I \in \mathbb{R}^{2 \times 2}$ and, hence, $P \in \mathbb{R}^{16 \times 16}$.